

A Generic Variational Framework for Demosaicking and Performance Analysis of Color Filter Arrays

Laurent Condat

GREYC Lab., Image Team, Caen, France
laurent.condat@greyc.ensicaen.fr

Abstract—We propose a novel method for image demosaicking from samples obtained with a completely arbitrary color filter array (CFA). We adopt a variational approach where the reconstructed image has maximal smoothness under the constraint of consistency with the available measurements. This optimization problem boils down to a large, sparse system of linear equations to solve, for which we propose an iterative algorithm. Although the proposed approach is linear, it yields visually pleasing demosaicked images and provides a robust framework for comparing the performances of CFAs.

Index Terms—Demosaicking, color filter array, variational reconstruction, regularized inverse problem

I. INTRODUCTION

At the heart of color imaging systems like digital cameras is a sensor on which a *color filter array* (CFA) is overlaid [1]. A CFA is a mosaic of color filters sensitive to only a portion of the visible light spectrum. The most popular CFA, used in a majority of digital cameras, is the Bayer CFA [2], that consists in red (R), green (G) and blue (B) filters arranged periodically. Given the mosaicked image acquired by the sensor, some processing is required to reconstruct a full color image with its three complete R,G,B channels. There is an extensive literature proposing solutions to this interpolation problem, called *demosaicking*—see e.g. [1], [3]–[10] and references therein—but in almost all works, acquisition with the Bayer CFA is assumed. In comparison, the design of other CFAs that would overcome the limitations of the latter—especially the aliasing effects in regions with horizontal or vertical high frequency content—has received little attention. Yet, the CFA is the most crucial element in a color imaging pipeline and even the best demosaicking algorithm can not recover the information lost because of the intrinsic limitations of the CFA. Although the design of new CFAs can be based on a theoretical analysis of their spectral properties [3], [4], [11], the need exists for a generic demosaicking method, in order to concretely compare them and to evaluate their performances. Such a method should be robust, applicable to all CFAs, while being independent of their specificities for a fair comparison between them. To our knowledge, only the demosaicking approach of Lukac *et al.* can be used to compare different

CFAs, under the important limitation that they consist of R,G, and B filters [12]. Recently, new promising CFA designs with filters having arbitrary colors were proposed [11]. In this work, we present a new demosaicking method which can be applied to arbitrary CFAs, without any constraint on the colors of their filters or their arrangement—periodic or on a random pattern. This method is linear, hence simple to implement, robust, and insensitive to biases due to the choice of *ad hoc* heuristics in non-linear methods. It also yields visually pleasant images, although it does not reach the quality of the best non-linear methods in the specific case of the Bayer pattern. However, we show that the image quality depends more on the CFA than on the demosaicking method used, which indicates that alternatives to the Bayer CFA should be considered seriously for use in the consumer market digital cameras.

Demosaicking is basically an ill-posed inverse problem, since only one linear measurement is available instead of three at every pixel. In this work, we regularize the demosaicking problem by adopting a variational approach and formulating the reconstruction as an optimization problem. Thus, we seek a solution that is consistent with the measurements, while minimizing a regularization term that penalizes the lack of smoothness. This way, the information contained in the available measurements is automatically filled in smoothly to surrounding pixels where information is missing. Although such a versatile formalism is classical in image processing and has been used for several problems, like interpolation [13] or reconstruction from non-uniform samples [14]–[16], its application to color images is new. The key point to exploit the statistical dependencies between the R, G and B channels in natural images is to express the smoothness term in the luminance-chrominance basis and to impose a smaller penalty to the energy of the luminance than to the one of the chrominance. This formulation naturally encompasses the hypothesis of locally constant hue, which is at the heart of several proposed demosaicking methods [6], [9], [10]. We define the reconstruction problem in the continuous domain, where the regularization is well posed, with all the corresponding advantages: the demosaicked image is simply obtained by resampling the reconstructed function, but the function may be eventually used for other tasks, or resampled at a different resolution. We seek a function lying in some uniform linear shift-invariant space, so that it is parameterized by discrete coefficients. Hence, the optimization problem boils down to a purely discrete problem, under the form of a large

This work was performed during the post-doctoral stay of the author at the Helmholtz Zentrum München — German Research Center for Environmental Health, Neuherberg, Germany, where he was supported by the Marie Curie Excellence Team Grant MEXT-CT-2004-013477, Acronym MAMEBIA, funded by the European Commission.

and sparse system of linear equations to solve. To this end, we propose a simple iterative algorithm that converges to a visually satisfying demosaicked image after a few number of iterations.

The paper is organized as follows. In Section II, we set up the variational reconstruction problem in the continuous domain and derive its solution, under the form of a system of linear equations. We propose in Section III an iterative algorithm for solving it and discuss the choice of the tuning parameters. We then give experimental results in Section IV, in order to establish a comparison between several CFAs.

A. Notations and Other Preliminaries

In this article, boldface letters denote vectors, e.g. $\mathbf{k} = [k_1, k_2]^T \in \mathbb{Z}^2$. A color is a vector of \mathbb{R}^3 and we define the canonical R,G,B basis of the color space by $\mathbf{R} = [1, 0, 0]^T$, $\mathbf{G} = [0, 1, 0]^T$, $\mathbf{B} = [0, 0, 1]^T$.

A color image is denoted by $\mathbf{g} = (\mathbf{g}[\mathbf{k}])_{\mathbf{k} \in \mathbb{Z}^2}$, where $\mathbf{g}[\mathbf{k}] \in \mathbb{R}^3$ is the color of the pixel centered at location $\mathbf{k} \in \mathbb{Z}^2$. We denote by g^R , g^G and g^B the components of \mathbf{g} in the R,G,B basis. A CFA \mathbf{h} is defined as a color image, with the additional constraint that $\mathbf{h}[\mathbf{k}] \in [0, 1]^3$ for every \mathbf{k} , for physical realizability of the filters.

We define in the following the color image \mathbf{u} as the ground truth to be estimated by the demosaicking process, while \mathbf{h} denotes the CFA used for the acquisition. The scalar pixel values $v[\mathbf{k}] \in \mathbb{R}$ of the mosaicked image v form the available data set from which we want to estimate \mathbf{u} . The acquisition process is modeled by the simple linear relationship:

$$v[\mathbf{k}] = \langle \mathbf{u}[\mathbf{k}], \mathbf{h}[\mathbf{k}] \rangle, \quad (1)$$

for every $\mathbf{k} \in \mathbb{Z}^2$, where we introduce the scalar product of two vectors, $\langle \mathbf{a}, \mathbf{b} \rangle = \mathbf{a}^T \mathbf{b}$.

It is well known that in natural images, the R,G,B components are not independent [1], [5], [7], [17]. Thus, we consider instead the orthonormal basis corresponding to luminance, red-green and blue-yellow chrominances, defined as

$$\mathbf{L} = \frac{1}{\sqrt{3}}[1, 1, 1]^T, \mathbf{C}_1 = \frac{1}{\sqrt{2}}[-1, 1, 0]^T, \mathbf{C}_2 = \frac{1}{\sqrt{6}}[-1, -1, 2]^T, \quad (2)$$

respectively. We denote g^L , g^{C_1} and g^{C_2} the components of a color image \mathbf{g} in this basis. These components can be considered as statistically independent [17]. According to the theory of opponent colors, validated by experimental evidences [18], this luminance/chrominance basis is also a good model for the three channels used in the human visual system to process the visual information. This may indicate that the evolution favored our biological visual system because it is adapted to the statistics of natural color scenes [19].

We define the \mathcal{Z} transform of a scalar filter $g = (g[\mathbf{k}])_{\mathbf{k} \in \mathbb{Z}^2}$ as $G(\mathbf{z}) = \sum_{\mathbf{k} \in \mathbb{Z}^2} g[\mathbf{k}] z_1^{-k_1} z_2^{-k_2}$ and we extend it to a vector filter \mathbf{g} by applying it component-wise. We also define the inverse filter \mathbf{g}^{-1} of \mathbf{g} as the filter with \mathcal{Z} transform $1/G(\mathbf{z})$.

We introduce the autocorrelation function a_φ of a function $\varphi(\mathbf{x})$ by $a_\varphi(\mathbf{x}) = (\varphi * \tilde{\varphi})(\mathbf{x})$, using the flip operator $\tilde{\varphi}(\mathbf{x}) = \varphi(-\mathbf{x})$.

II. VARIATIONAL RECONSTRUCTION

A. Formulation of the Problem

Given the mosaicked image $v = \langle \mathbf{u}, \mathbf{h} \rangle$ acquired using a given CFA \mathbf{h} , the demosaicking process aims at reconstructing a demosaicked image $\tilde{\mathbf{u}}$, that is a good estimate of the unknown ground truth \mathbf{u} .

A natural criterion to be satisfied by $\tilde{\mathbf{u}}$ is the consistency [20] with respect to the mosaicked image, that is,

$$v = \langle \tilde{\mathbf{u}}, \mathbf{h} \rangle. \quad (3)$$

With consistency only, demosaicking is obviously an ill-posed problem. The solution we adopt in this work consists, at least formally, in reconstructing a continuously-defined function $\tilde{\mathbf{f}} : \mathbb{R}^2 \mapsto \mathbb{R}^3$, that is then resampled to yield the demosaicked image:

$$\tilde{\mathbf{u}}[\mathbf{k}] = \tilde{\mathbf{f}}(\mathbf{k}), \quad \forall \mathbf{k} \in \mathbb{Z}^2. \quad (4)$$

We regularize the problem and look for the function that minimizes some quadratic functional, under the consistency constraint:

$$\tilde{\mathbf{f}} = \underset{\mathbf{g} \in \Omega}{\operatorname{argmin}} \mathcal{Q}(\mathbf{g}), \quad \text{s.t.} \quad \langle \mathbf{g}(\mathbf{k}), \mathbf{h}[\mathbf{k}] \rangle = v[\mathbf{k}] \quad \forall \mathbf{k} \in \mathbb{Z}^2, \quad (5)$$

for some functional space Ω to be chosen. Popular functionals used in signal and image processing, approximation theory, or statistics, penalize the lack of smoothness of the solution [15], [16]. Of particular interest are Duchon's semi-norms, which are invariant under rotations, defined for a scalar function $g(\mathbf{x})$ as [21],

$$\mathcal{M}_p(g) = \int_{\mathbb{R}^2} \|D^p g(\mathbf{x})\|^2 d\mathbf{x}, \quad (6)$$

where D^p is the vector of all possible partial derivative operators of order p . For instance,

$$\mathcal{M}_1(g) = \int_{\mathbb{R}^2} \left(\frac{\partial g(\mathbf{x})}{\partial x_1} \right)^2 + \left(\frac{\partial g(\mathbf{x})}{\partial x_2} \right)^2 d\mathbf{x}, \quad (7)$$

$$\mathcal{M}_2(g) = \int_{\mathbb{R}^2} \left(\frac{\partial^2 g(\mathbf{x})}{\partial x_1^2} \right)^2 + 2 \left(\frac{\partial^2 g(\mathbf{x})}{\partial x_1 \partial x_2} \right)^2 + \left(\frac{\partial^2 g(\mathbf{x})}{\partial x_2^2} \right)^2 d\mathbf{x}. \quad (8)$$

For the reconstruction of color images, we have to define a smoothness functional that can be applied to vector-valued functions. Since we assumed that the luminance and chrominance components of natural scenes are independent, we adopt a functional that is diagonal in the luminance/chrominance basis, using Duchon's semi-norms on each component:

$$\mathcal{Q}_{p,\mu}(\mathbf{g}) = \mu \mathcal{M}_p(g^L) + \mathcal{M}_p(g^{C_1}) + \mathcal{M}_p(g^{C_2}), \quad (9)$$

for some integer order $p \geq 1$ and weight parameter $\mu > 0$. This functional is rotation-invariant with respect to the spatial variable \mathbf{x} , but also invariant with respect to a rotation in the color plane of the color value of \mathbf{g} : if

$$[g_\theta^L, g_\theta^{C_1}, g_\theta^{C_2}]^T = \begin{pmatrix} 1 & 0 & 0 \\ 0 & \cos(\theta) & -\sin(\theta) \\ 0 & \sin(\theta) & \cos(\theta) \end{pmatrix} [g^L, g^{C_1}, g^{C_2}]^T, \quad (10)$$

then $\mathcal{Q}_{p,\mu}(\mathbf{g}_\theta) = \mathcal{Q}_{p,\mu}(\mathbf{g})$, for every $\theta \in \mathbb{R}$. Thus, there is no privileged color axis and the smoothness of the chrominance is penalized in a fair way in every iso-luminant color plane.

With this functional, the optimization problem (5) is well posed: there exists a solution, since the space of consistent reconstructions is not empty, and the solution is unique due to the convexity of $\mathcal{Q}_{p,\mu}$.

The parameter μ in (9) plays a crucial role in our formulation. It controls the balance between the smoothness of the luminance and the smoothness of the chrominance for the reconstructed function. Qualitatively, we can remark that

- If $\mu = 0$, then the solution of the problem (5) is not unique and corresponds to a gray-scale function plus a color constant: every function of the form $\tilde{\mathbf{f}}(\mathbf{x}) = f(\mathbf{x})\mathbf{L} + \mathbf{C}$ for some scalar function f and color $\mathbf{C} \in \mathbb{R}^3$, which is consistent with the mosaicked samples, is solution of (5), since it is in the null space of $\mathcal{Q}_{p,0}$. For instance, the gray-scale demosaicked image defined by $\tilde{\mathbf{u}}[\mathbf{k}] = (v[\mathbf{k}]/h^L[\mathbf{k}])\mathbf{L}$ for every \mathbf{k} , is a valid solution, in which all the available information has been assigned to the luminance. This trivial solution is clearly not satisfying.
- If $\mu = 1$, we can rewrite $\mathcal{Q}_{p,1}$ in the R,G,B basis as $\mathcal{Q}_{p,1}(\mathbf{g}) = \mathcal{M}_p(g^R) + \mathcal{M}_p(g^G) + \mathcal{M}_p(g^B)$. Hence, for a CFA with R,G,B filters, the demosaicking process amounts to reconstruct the R,G,B channels independently, and the global solution to (5) is obtained by interpolation of each channel using thin-plate splines [21]. For the Bayer CFA and $p = 1$, the solution will be very close to what is obtained by bilinear interpolation. Thus, the case $\mu = 1$ is not satisfying, neither, since it does not take into account the cross-correlations between the R,G,B channels.

Consequently, μ should be chosen between 0 and 1, and relatively small in order to get a slowly varying hue across the image. However, a too small value will produce watercolor effects at sharp color transitions and, at the limit, a gray-scale image. Like often with tradeoff parameters, there is no mathematical rule for choosing μ , and the best value for a given CFA should be chosen empirically by trial and error, to give the best performances on test images.

B. Reconstruction in Shift-Invariant Spaces

For the problem to be completely defined, we have to choose the reconstruction space Ω in (5). Finding the analytical form of the global minimizer of (5) among all possible functions (more rigorously, in the Sobolev space of order p) is a too complicated problem. We can expect the solution to be expressed in the basis of some ‘‘colored’’ thin-plate splines shifted at every pixel of the lattice \mathbb{Z}^2 , similarly to the scalar case [21]. For the practical purpose of image demosaicking we focus on in this paper, an extensive mathematical treatment of this solution is not required.

Instead, we constrain the reconstruction space Ω to be a linear shift-invariant (LSI) space [22], [23] \mathcal{V}_φ generated by

some function φ to be chosen:

$$\mathcal{V}_\varphi = \left\{ \mathbf{g}(\mathbf{x}) = \sum_{\mathbf{k} \in \mathbb{Z}^2} \mathbf{c}[\mathbf{k}] \varphi(\mathbf{x} - \mathbf{k}) \quad : \quad \mathbf{c}[\mathbf{k}] \in \mathbb{R}^3 \quad \forall \mathbf{k} \right\}. \quad (11)$$

LSI spaces have been used extensively in sampling theory, for approximation and interpolation [24], and they are at the heart of the wavelet theory. The function φ can be chosen arbitrarily, under the following assumptions:

- φ is bounded with compact support. This condition is not necessary, but we enforce it for implementation purpose.
- The shifts $\varphi(\mathbf{x} - \mathbf{k})$ form a Riesz basis of $\mathcal{V}_\varphi \cap L_2$ [22], so that each function $\mathbf{g} \in \mathcal{V}_\varphi$ has a unique expansion in the form (11).
- $\mathcal{M}_p(\varphi) < +\infty$ so that the smoothness term $\mathcal{Q}_{p,\mu}(\mathbf{g})$ does not blow up for every $\mathbf{g} \in \mathcal{V}_\varphi$.

In practical reconstruction problems encountered in image processing, spline spaces have shown to be particularly adequate [15], [24], [25]. In that case, φ is chosen as the separable centered B-spline β^d of degree $d \geq p$ [25].

Thus, our reconstruction problem boils down to finding the coefficients $\mathbf{c}[\mathbf{k}] \in \mathbb{R}^3$ that parameterize the function

$$\tilde{\mathbf{f}}(\mathbf{x}) = \sum_{\mathbf{k} \in \mathbb{Z}^2} \mathbf{c}[\mathbf{k}] \varphi(\mathbf{x} - \mathbf{k}), \quad (12)$$

so that $\tilde{\mathbf{f}}$ is solution of (5) with $\Omega = \mathcal{V}_\varphi$.

C. Derivation of the Solution

We now express the solution of the minimization problem in terms of the pixel values $\tilde{\mathbf{u}}[\mathbf{k}]$ of the demosaicked image. The consistency is expressed by (3). In order to discretize the variational term, we first remark that $D^p \varphi(-\mathbf{x}) = (-1)^p D^p \varphi(\mathbf{x})$. Consequently, we obtain

$$\mathcal{Q}_{p,\mu}(\tilde{\mathbf{f}}) = \quad (13)$$

$$\sum_{\mathbf{k}, \mathbf{l} \in \mathbb{Z}^2} \left(\mu c^L[\mathbf{k}] c^L[\mathbf{l}] + c^{C_1}[\mathbf{k}] c^{C_1}[\mathbf{l}] + c^{C_2}[\mathbf{k}] c^{C_2}[\mathbf{l}] \right) \times \int_{\mathbb{R}^2} D^p \varphi(\mathbf{x} - \mathbf{k})^T D^p \varphi(\mathbf{x} - \mathbf{l}) d\mathbf{x} = \quad (14)$$

$$\sum_{\mathbf{k}, \mathbf{l} \in \mathbb{Z}^2} \left(\mu c^L[\mathbf{k}] c^L[\mathbf{l}] + c^{C_1}[\mathbf{k}] c^{C_1}[\mathbf{l}] + c^{C_2}[\mathbf{k}] c^{C_2}[\mathbf{l}] \right) \times (-1)^p ((D^p)^T D^p a_\varphi)(\mathbf{k} - \mathbf{l}) = \quad (15)$$

$$\mu \sum_{\mathbf{k} \in \mathbb{Z}^2} c^L[\mathbf{k}] (c^L * q_{\varphi,p})[\mathbf{k}] + \sum_{\mathbf{k} \in \mathbb{Z}^2} c^{C_1}[\mathbf{k}] (c^{C_1} * q_{\varphi,p})[\mathbf{k}] + \sum_{\mathbf{k} \in \mathbb{Z}^2} c^{C_2}[\mathbf{k}] (c^{C_2} * q_{\varphi,p})[\mathbf{k}], \quad (16)$$

where $q_{\varphi,p}$ is the discrete filter defined by

$$q_{\varphi,p}[\mathbf{k}] = (-1)^p ((D^p)^T D^p a_\varphi)(\mathbf{k}) \quad (17)$$

$$= (-1)^p \sum_{a+b=p} \binom{p}{a} \frac{\partial^{2p} a_\varphi(\mathbf{x})}{\partial x_1^{2a} \partial x_2^{2b}} \Big|_{\mathbf{x}=\mathbf{k}} \quad (18)$$

for every $\mathbf{k} \in \mathbb{Z}^2$. In the case where φ is a separable B-spline, explicit formulas for the filters $q_{\varphi,p}$ have been given in [15]. In the most simple case corresponding to bilinear reconstruction

(φ is the separable centered B-spline of degree 1) and $p = 1$, the filter is

$$q_{\beta^1,1} = \frac{1}{3} \begin{bmatrix} -1 & -1 & -1 \\ -1 & 8 & -1 \\ -1 & -1 & -1 \end{bmatrix}. \quad (19)$$

In order to express the minimization problem in terms of $\tilde{\mathbf{u}}$ instead of \mathbf{c} , we define b_φ as the discretization of φ by $b_\varphi[\mathbf{k}] = \varphi(\mathbf{k})$ for every $\mathbf{k} \in \mathbb{Z}^2$. Then,

$$\mathbf{c} = \tilde{\mathbf{u}} * b_\varphi^{-1}. \quad (20)$$

Thus, we obtain the final form

$$\mathcal{Q}_{p,\mu}(\tilde{\mathbf{f}}) = \mu \langle \tilde{u}^L, \tilde{u}^L * r_{\varphi,p} \rangle + \langle \tilde{u}^{C_1}, \tilde{u}^{C_1} * r_{\varphi,p} \rangle + \langle \tilde{u}^{C_2}, \tilde{u}^{C_2} * r_{\varphi,p} \rangle, \quad (21)$$

where we introduce the filter $r_{\varphi,p} = q_{\varphi,p} * (b_\varphi)^{-1} * (\bar{b}_\varphi)^{-1}$.

When minimizing a quadratic criterion under a linear constraint, it is well known that the solution can be derived by expressing the associated Lagrangian criterion [26]. In our case,

$$\mathcal{C}(\tilde{\mathbf{f}}) = \mathcal{Q}_{p,\mu}(\tilde{\mathbf{f}}) + 2 \sum_{\mathbf{k} \in \mathbb{Z}^2} \lambda[\mathbf{k}] \left(\langle \tilde{\mathbf{u}}[\mathbf{k}], \mathbf{h}[\mathbf{k}] \rangle - v[\mathbf{k}] \right). \quad (22)$$

Then, the desired solution is obtained by setting the partial derivatives of \mathcal{C} to zero, with respect to the unknowns $\tilde{u}^L[\mathbf{k}]$, $\tilde{u}^{C_1}[\mathbf{k}]$, $\tilde{u}^{C_2}[\mathbf{k}]$, and the Lagrangian parameters $\lambda[\mathbf{k}]$. Thus, we obtain the following set of linear equations, that describe the solution of our problem: for every $\mathbf{k} \in \mathbb{Z}^2$,

$$\begin{cases} \mu (\tilde{u}^L * r_{\varphi,p})[\mathbf{k}] + \lambda[\mathbf{k}] h^L[\mathbf{k}] = 0, \\ (\tilde{u}^{C_1} * r_{\varphi,p})[\mathbf{k}] + \lambda[\mathbf{k}] h^{C_1}[\mathbf{k}] = 0, \\ (\tilde{u}^{C_2} * r_{\varphi,p})[\mathbf{k}] + \lambda[\mathbf{k}] h^{C_2}[\mathbf{k}] = 0, \\ \tilde{u}^L[\mathbf{k}] h^L[\mathbf{k}] + \tilde{u}^{C_1}[\mathbf{k}] h^{C_1}[\mathbf{k}] + \tilde{u}^{C_2}[\mathbf{k}] h^{C_2}[\mathbf{k}] = v[\mathbf{k}]. \end{cases} \quad (23)$$

In the next Section, we propose an iterative algorithm to solve this system of equations.

III. PRACTICAL DEMOSAICKING METHOD

A. Iterative Demosaicking Algorithm

Since the linear system (23) does not have a simple sparse form that would provide us with a direct solution, we propose an iterative scheme that converges to the solution. Formally, the method is a so-called Jacobi iterator, that approximates the inverse of the convolution matrix corresponding to $r_{\varphi,p}$ by the inverse of its diagonal [27]. That is, each refinement step updates the demosaicked image as follows: for every $\mathbf{k} \in \mathbb{Z}^2$,

$$\tilde{u}_{(n)}^L[\mathbf{k}] = \tilde{u}_{(n-1)}^L[\mathbf{k}] - 1/r_{\varphi,p}[\mathbf{0}] \times \left((\tilde{u}_{(n-1)}^L * r_{\varphi,p})[\mathbf{k}] + \lambda_{(n)}[\mathbf{k}] h^L[\mathbf{k}]/\mu \right), \quad (24)$$

$$\tilde{u}_{(n)}^{C_1}[\mathbf{k}] = \tilde{u}_{(n-1)}^{C_1}[\mathbf{k}] - 1/r_{\varphi,p}[\mathbf{0}] \times \left((\tilde{u}_{(n-1)}^{C_1} * r_{\varphi,p})[\mathbf{k}] + \lambda_{(n)}[\mathbf{k}] h^{C_1}[\mathbf{k}] \right), \quad (25)$$

$$\tilde{u}_{(n)}^{C_2}[\mathbf{k}] = \tilde{u}_{(n-1)}^{C_2}[\mathbf{k}] - 1/r_{\varphi,p}[\mathbf{0}] \times \left((\tilde{u}_{(n-1)}^{C_2} * r_{\varphi,p})[\mathbf{k}] + \lambda_{(n)}[\mathbf{k}] h^{C_2}[\mathbf{k}] \right), \quad (26)$$

where $X_{(n)}$ denotes the value of the quantity X after the n -th iteration. Then, according to this scheme, we can rewrite the linear system (23) as the following one, where the unknowns are spatially de-interlaced. We first assume that the regularization filter is normalized such that $r_{\varphi,p}[\mathbf{0}] = 1$, which is not restrictive. Then, our iterative algorithm boils down to solving, during each iteration and for each \mathbf{k} in scanline order in the image, a 4×4 linear system in terms of the unknowns $\tilde{u}_{(n)}^L[\mathbf{k}]$, $\tilde{u}_{(n)}^{C_1}[\mathbf{k}]$, $\tilde{u}_{(n)}^{C_2}[\mathbf{k}]$, $\lambda_{(n)}[\mathbf{k}]$:

$$\begin{cases} \tilde{u}_{(n)}^L[\mathbf{k}] + \lambda_{(n)}[\mathbf{k}] h^L[\mathbf{k}]/\mu = (\tilde{u}_{(n-1)}^L * r'_{\varphi,p})[\mathbf{k}], \\ \tilde{u}_{(n)}^{C_1}[\mathbf{k}] + \lambda_{(n)}[\mathbf{k}] h^{C_1}[\mathbf{k}] = (\tilde{u}_{(n-1)}^{C_1} * r'_{\varphi,p})[\mathbf{k}], \\ \tilde{u}_{(n)}^{C_2}[\mathbf{k}] + \lambda_{(n)}[\mathbf{k}] h^{C_2}[\mathbf{k}] = (\tilde{u}_{(n-1)}^{C_2} * r'_{\varphi,p})[\mathbf{k}], \\ \tilde{u}_{(n)}^L[\mathbf{k}] h^L[\mathbf{k}] + \tilde{u}_{(n)}^{C_1}[\mathbf{k}] h^{C_1}[\mathbf{k}] + \tilde{u}_{(n)}^{C_2}[\mathbf{k}] h^{C_2}[\mathbf{k}] = v[\mathbf{k}]. \end{cases} \quad (27)$$

where $r'_{\varphi,p} = \delta_0 - r_{\varphi,p}$ and δ_0 is the identity filter with \mathcal{Z} transform equal to 1. For given n and \mathbf{k} , this linear system is solved by first calculating $\lambda_{(n)}[\mathbf{k}]$ and then updating the pixel values of the demosaicked image using the first three equations of the system (27). $\lambda_{(n)}[\mathbf{k}]$ is computed using the following equality, derived by substitutions in the system:

$$\lambda_{(n)}[\mathbf{k}] (h^L[\mathbf{k}]^2/\mu + h^{C_1}[\mathbf{k}]^2 + h^{C_2}[\mathbf{k}]^2) = h^L[\mathbf{k}] (\tilde{u}_{(n-1)}^L * r'_{\varphi,p})[\mathbf{k}] + h^{C_1}[\mathbf{k}] (\tilde{u}_{(n-1)}^{C_1} * r'_{\varphi,p})[\mathbf{k}] + h^{C_2}[\mathbf{k}] (\tilde{u}_{(n-1)}^{C_2} * r'_{\varphi,p})[\mathbf{k}] - v[\mathbf{k}]. \quad (28)$$

We note that the consistency is satisfied exactly by the demosaicked image $\tilde{\mathbf{u}}_{(n)}$ after each iteration. Thus, even only one iteration could be used as post-processing to improve the result of another demosaicking algorithm that would yield visually pleasing but not consistent demosaicked images.

The complexity of our algorithm is about three convolutions with $r_{\varphi,p}$ at each iteration. The method proposed in this article is based on the most simple iterator for solving large linear systems; it is stable, efficient, and easy to implement, but the convergence may be slow. So, our algorithm is not particularly competitive with respect to the computation time. More complex schemes could be used to improve the speed of convergence: Gauss-Seidel iterator or other descent methods of convex optimization, introduction of damping parameters. . . Such refinements are left to the interested practitioners, however.

The proposed algorithm is also versatile in the sense that it can handle the situation when the sensor has ‘‘dead pixels’’, that is, the value $v[\mathbf{k}]$ is corrupted and irrelevant for some \mathbf{k} . In that case, simply set $\lambda_{(n)}[\mathbf{k}] = 0$ during the computation of $\tilde{\mathbf{u}}_{(n)}[\mathbf{k}]$. This way, the value of the dead pixels are defined so that the smoothness of the image in their neighborhood is maximal; thus, the dead pixels should be invisible in the demosaicked image.

The sequel of the section is dedicated to the choice of the tuning parameters, namely the initial estimate $\tilde{\mathbf{u}}_{(0)}$, the stopping condition of the algorithm, the value of μ and the choice of $r_{\varphi,p}$.

B. Choice of the Parameters

We first remark that the proposed approach turns out to be discrete, since it depends on the discrete filter $r_{\varphi,p}$ only,

although formally a continuous model $\tilde{\mathbf{f}}$ is fitted on the demosaicked image. Actually, formulating the minimization problem in the LSI space \mathcal{V}_φ yields a reversal in its interpretation: instead of looking for a function that depends on the measurements only and that is then resampled on the target lattice \mathbb{Z}^2 , we look for the demosaicked image $\tilde{\mathbf{u}}$ such that the function $\tilde{\mathbf{f}}$ that interpolate it, defined by means of (12) and (20), has maximal smoothness. Thus, for the task of demosaicking only, the function $\tilde{\mathbf{f}}$ does not come into play directly; the continuous formalism only provides a well-suited design method for the regularization filter $r_{\varphi,p}$. However, if the demosaicked image is interpolated for further treatment or resampling, we have the guarantee that the underlying model $\tilde{\mathbf{f}}(\mathbf{x})$ is satisfying, with respect to the smoothness prior.

We implemented the method using a linear spline model, with $\varphi = \beta^1$ and $p = 1$, and a cubic spline model, with $\varphi = \beta^3$ and $p = 2$. In this second case, the filter $q_{\varphi,p}$ is a 7×7 filter given in [15, Tab. 1]. We note that the computation of the value $r_{\beta^3,2}[\mathbf{0}]$, which is required in our implementation, is not trivial. We obtained this value by noticing that

$$r_{\varphi,p}[\mathbf{0}] = \frac{1}{4\pi^2} \int_{[-\pi,\pi]^2} \frac{\sum_{\mathbf{k} \in \mathbb{Z}^2} q_{\varphi,p}[\mathbf{k}] e^{-j\omega^T \mathbf{k}}}{\left| \sum_{\mathbf{k} \in \mathbb{Z}^2} \varphi(\mathbf{k}) e^{-j\omega^T \mathbf{k}} \right|^2} d\omega, \quad (29)$$

which can be calculated exactly. For instance, $r_{\beta^3,2}[\mathbf{0}] = (14766 - 175\sqrt{3})/175$. We also tried the regularization filter

$$r_0 = \frac{1}{4} \begin{bmatrix} 0 & -1 & 0 \\ -1 & 4 & -1 \\ 0 & -1 & 0 \end{bmatrix}. \quad (30)$$

The filter r_0 is not derived from some function φ and order p , which means that when using this filter, the continuous interpretation associated to the method is lost. It turned out in our experiments that, independently of the CFA chosen, r_0 provides the best performance among the three tested regularization filter. After mosaicking and demosaicking the test images used for our experiments (see in Section IV), the average mean-square-error with r_0 is roughly 95% that with $r_{\beta^3,2}$ and 89% that with $r_{\beta^1,1}$. Thus, we adopt the filter r_0 as the regularization filter to be used in our framework, since it provides the best results for the minimal complexity.

Since the solution of the problem is unique, it does not depend on the estimate $\tilde{\mathbf{u}}_{(0)}$ that serves as initialization for the iterative algorithm. However, the choice of $\tilde{\mathbf{u}}_{(0)}$ influences the speed of convergence. The gray-scale image $\tilde{\mathbf{u}}_{(0)}[\mathbf{k}] = (v[\mathbf{k}]/h^L[\mathbf{k}]) \cdot \mathbf{1}$ is not a good initializer since the color information is then very slowly recovered. The consistent color mosaicked image $\tilde{\mathbf{u}}_{(0)}[\mathbf{k}] = (v[\mathbf{k}]/\|\mathbf{h}[\mathbf{k}]\|^2) \cdot \mathbf{h}[\mathbf{k}]$ is also a bad initializer, because the average color of the CFA (e.g., greenish for the Bayer pattern) disappears very slowly along the iterations (a color constant is in the kernel of the smoothness penalty term). A method that turns out to work well in practice consists in starting with a uniform grey image $\tilde{\mathbf{u}}_{(0)}[\mathbf{k}] = 127.5$ and in performing a few iterations (we used 10 iterations) with the parameter $\mu = 1$. Thus, the spatial distribution of the color information is roughly but quickly recovered and the repartition of the high frequency content between the

luminance and chrominance channels is then refined by the subsequent iterations with the correct value of μ .

As mentioned at the end of Section II-A, there is no definite rule for choosing the important parameter μ . The value giving the best results depends on the image and on the CFA considered. For the seven CFAs compared in this article, depicted in Fig. 1 and detailed in the next section, we found out that the value $\mu = 0.04$ provides good results for the CFAs (I) to (IV), while $\mu = 0.11$ is better for the CFAs (V) to (VII), which have a higher light sensitivity (average value of $h^L[\mathbf{k}]$ over \mathbf{k}). These values were roughly determined by empirical trials, considering the minimization of the mean squared error (MSE) averaged over the twenty images used for the experiments in the next section. These values are indicative only, but it turns out that the best value for a given CFA closely depends on the ratio between its color discrimination capabilities and its light sensitivity, although this notion is hard to quantify.

The convergence of the proposed iterative algorithm is relatively slow, that is, up to thousand iterations have to been run before the solution is achieved up to machine precision. The convergence turns out to be faster for the RGB CFAs than for CFAs with higher light sensitivity. But surprisingly, when observing for a given image the MSE with respect to the ground-truth along the iterations, we found that it achieves a minimum after a few iterations only, after increasing progressively toward the MSE of the asymptotic solution. This statement does not hold for every CFA, however, and it may depend on the filter $r_{\varphi,p}$ and value of μ adopted. Anyhow, for the tests in the next section, we ran only 19 iterations of the algorithm—including the 10 iterations for the initialization with $\mu = 1$ as detailed previously—for the CFAs (I) to (V). Here also, this choice is empirical and the number of iterations giving the best result depends on the image considered. For the CFAs (VI) and (VII), we did not observe this behavior and the MSE decreases monotonically along the iterations; so, 100 iterations were ran to yield the results reported in Tab. I.

IV. PRACTICAL COMPARISON OF THE PERFORMANCES OF CFAS

In order to validate our method experimentally, we considered the data set of 20 color images of size 768×512 used by many authors to test their methods (e.g. [8], [11]). These images were mosaicked using several CFAs and demosaicked using our method, with the values of the tuning parameters as discussed in Section III-B. The mean squared errors (MSE)¹ obtained are reported in Tab. I. The CFA considered in this comparison, which are depicted in Fig. 1 are:

- (I). The well-known Bayer CFA [2].

¹The MSE for an image of size $N \times M$ is

$$\frac{1}{3NM} \sum_{\mathbf{k} \in [1..N] \times [1..M]} |u^R[\mathbf{k}] - \tilde{u}^R[\mathbf{k}]|^2 + |u^G[\mathbf{k}] - \tilde{u}^G[\mathbf{k}]|^2 + |u^B[\mathbf{k}] - \tilde{u}^B[\mathbf{k}]|^2. \quad (31)$$

However, in this article, we do not take into account the first and last three rows and columns of the demosaicked images for the computation of the MSE, since the initial images used for the tests have been badly acquired at the boundaries.

TABLE I

MEAN SQUARED ERROR FOR THE DEMOSAICKING EXPERIMENTS USING THE CFAs (I) TO (VII) AND THE PROPOSED DEMOSAICKING METHOD. IMAGE NUMBERS CORRESPOND TO [8]. THE LAST ROW GIVES THE AVERAGE OVER THE 20 IMAGES.

Image	(I)	(II)	(III)	(IV)	(V)	(VI)	(VII)
1	13.76	12.92	11.58	11.17	17.13	24.36	11.12
2	14.79	13.20	11.61	13.10	19.80	16.10	15.52
3	18.84	20.36	22.36	20.10	23.75	37.41	22.71
4	12.06	11.61	9.45	8.64	11.58	17.85	9.03
5	8.06	7.94	7.78	8.08	10.25	12.15	9.40
6	31.97	20.56	19.31	17.80	35.13	43.06	18.41
7	6.65	6.15	6.11	5.60	7.48	10.10	7.10
8	5.62	6.01	6.05	5.69	6.61	10.06	5.91
9	10.66	10.27	9.85	9.21	11.93	17.38	10.40
10	5.62	5.49	4.62	5.01	7.93	7.39	5.06
11	20.99	22.80	26.76	20.61	20.41	45.32	23.52
12	12.55	11.43	10.84	11.59	16.86	16.09	11.51
13	5.65	5.48	3.99	3.97	5.79	7.46	4.27
14	5.84	5.94	6.21	5.93	5.19	8.98	5.66
15	15.56	16.95	17.34	16.26	15.75	26.32	16.40
16	11.23	8.29	7.72	6.68	10.54	16.30	7.25
17	8.86	8.94	8.06	8.33	8.01	12.23	8.73
18	10.56	10.31	9.83	8.54	11.02	19.20	9.97
19	14.66	13.85	13.49	13.35	14.70	19.40	13.33
20	23.52	23.81	26.22	23.35	21.13	33.58	22.25
average	12.87	12.11	11.96	11.15	14.05	20.04	11.88

- (II). The R,G,B pattern proposed by Lukac in [12].
- (III). The random pattern of type 2 proposed by the author in [28]. Contrary to the other patterns, this one is aperiodic.
- (IV). A new pattern proposed in this work with R,G,B and Y (yellow) filters designed so that the filters for each of the four colors are arranged on a hexagonal lattice.
- (V). The CMY pattern with C (cyan), M (magenta) and Y filters, a variant of the Bayer CFA with doubled light sensitivity [2]. To our knowledge, this CFA has been neglected and no advanced demosaicking method has been proposed for it in the literature.
- (VI). One of the three new patterns recently proposed and patented by Kodak [29], that should be used in the next generation of digital cameras of this company for the consumer market. These new CFAs will replace the Bayer CFA, whose patent is also hold by Kodak. Thus, the development of demosaicking methods for this CFA will become an important problem in image processing in the near future.
- (VII). The pattern of type 1 recently designed by Hirakawa *et al.*, with better spectral properties than previous designs [11]. It consists in filters with the colors $[\frac{1}{2}, 1, 0]$, $[0, 1, \frac{1}{2}]$, $[1, 0, \frac{1}{2}]$ and $[\frac{1}{2}, 0, 1]$ arranged with a 4×2 periodicity.

For the CFAs (I) to (III) having R,G,B filters, we compared our method to two other demosaicking techniques:

- We propose a simple linear scheme that consists in computing a missing value for the color $C \in \{R,G,B\}$ at location \mathbf{k} , by averaging the pixel values $v[l]$ for l in a 3×3 neighborhood surrounding \mathbf{k} such that $h[l] = C$. This simple scheme reverts to bilinear interpolation for the Bayer pattern.
- We implemented the non-linear universal demosaicking

TABLE II

MEAN SQUARED ERROR FOR THE DEMOSAICKING EXPERIMENTS USING DIFFERENT COMBINATIONS OF R,G,B CFAs AND DEMOSAICKING METHODS. IMAGE NUMBERS CORRESPOND TO [8].

Image	Bayer (I)		Lukac (II)		random (III)	
	bilinear	[30]	bilinear	[30]	bilinear	[30]
1	154.92	16.26	155.39	21.54	143.56	22.96
2	31.75	7.61	31.48	8.89	30.29	9.42
3	139.59	15.61	146.20	22.50	146.73	32.26
4	109.32	12.81	110.05	17.59	103.76	17.35
5	29.14	5.06	29.84	7.29	30.56	8.22
6	283.68	33.14	276.64	31.41	251.86	37.91
7	36.87	5.19	37.03	7.11	35.24	7.66
8	37.18	4.96	39.21	7.09	37.08	8.38
9	77.44	9.40	77.93	11.89	74.84	14.41
10	31.44	4.85	31.98	6.80	29.58	5.93
11	264.32	27.94	269.93	34.02	266.70	49.84
12	43.85	9.05	43.96	10.33	42.44	11.63
13	47.25	5.95	47.62	8.12	44.03	7.24
14	40.71	5.49	41.61	7.05	41.38	9.40
15	105.51	15.14	107.46	18.69	104.10	24.50
16	103.26	11.34	99.86	11.00	90.45	14.27
17	44.41	6.33	45.66	8.47	44.89	10.27
18	90.56	10.86	91.54	14.08	88.23	16.28
19	57.95	12.18	58.19	13.87	56.15	15.63
20	138.68	24.64	141.76	27.97	139.48	35.56
average	93.39	12.19	94.17	14.79	90.07	17.96

algorithm of Lukac *et al.* [30] which is, to our knowledge, the only advanced demosaicking algorithm proposed in the literature, that can be used for every R,G,B CFA.

The MSE results are reported in Tab. II. We observe that the simple bilinear method, that does not exploit the cross-correlations between the color bands in natural images, provides poor results. Although our method is simple and linear, it outperforms the non-linear method of Lukac, except for the Bayer CFA. This may indicate that the latter has been designed to perform well with the Bayer CFA in particular.

In the specific case of the Bayer pattern, our linear approach does not compete with the many sophisticated non-linear methods proposed in the literature. To our knowledge, the best demosaicking technique proposed to date is the one of Dubois [4], with an average MSE over our 20 test images equal to 8.63². Another recent algorithm yields an average MSE equal to 9.28³ [31]. These values give an idea of the margin of improvement that could be expected, if non-linear methods were developed for each CFA to exploit at best their intrinsic performances. Also, they show that our approach is not so far from the best methods, if we compare with the results obtained by the naive bilinear interpolation in Tab. II.

As a result of Tab. I, we first observe that the choice of the CFA yields important differences. This confirms that the CFA is a crucial element in the color imaging pipeline and has to be carefully chosen. But on the other hand, there is no CFA that is better on all images and the comparison of the average MSE has to be relativized by the variance of the results from one image to another one. Interestingly, the best average MSE

²We computed the MSE using the images available online at <http://www.site.uottawa.ca/~edubois/demosaicking/>

³We performed the demosaicking experiments using the Matlab code put available online by the authors at <http://www.ntu.edu.sg/home5/CHAN0069/AFdemosaick.zip>

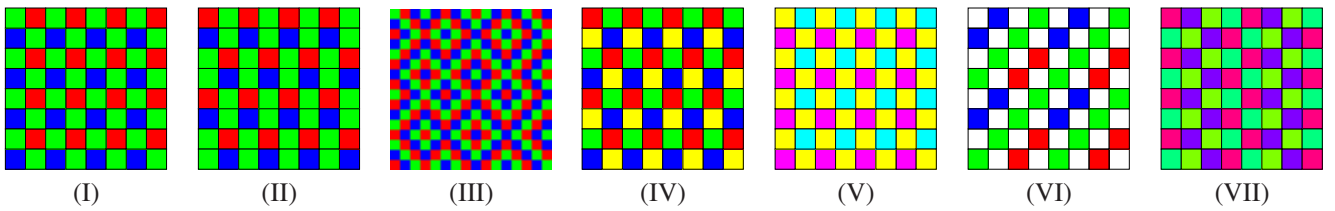


Fig. 1. The seven CFAs used in our experiments. (I): Bayer pattern [2], (II): Lukac pattern [12], (III): random pattern [28], (IV): new RGBY pattern, (V): CMY pattern [2], (VI): Kodak pattern [29], (VII): Hirakawa pattern [11].

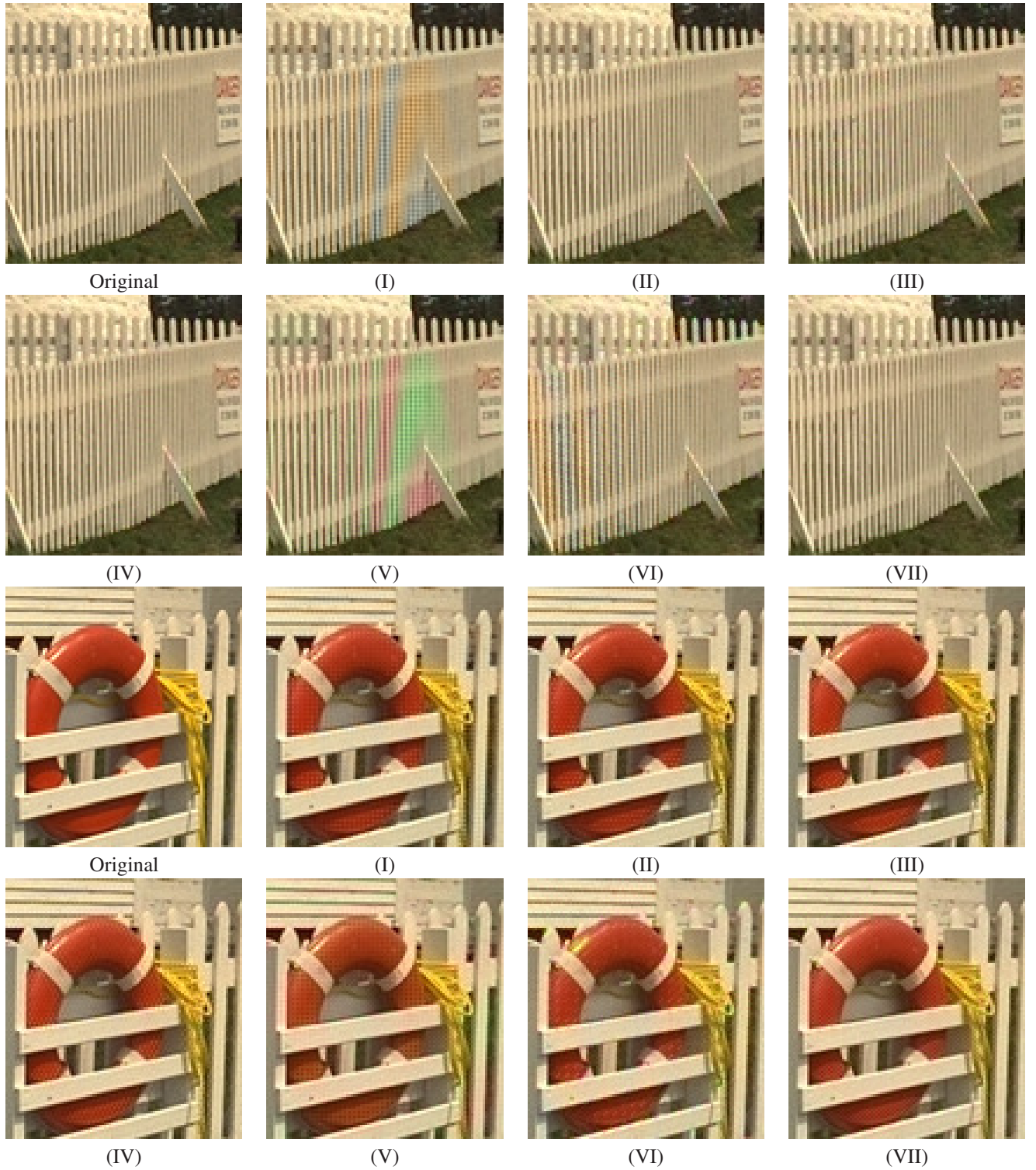


Fig. 2. Results of our demosaicing method used with the seven CFAs depicted in Fig. 1, on two parts of the *Lighthouse* image (image number 16 in Tab. I).

is obtained for our new CFA (IV), which was not expected at all. It is better than the second one, the CFA (VII), for 15 of the 20 images. However, we have to be cautious with this ranking, since the MSE results reported in [11] for the CFA (VII), using demosaicking by spectral selection, are the best reported ever. This indicates that the joint optimization of the CFA and the demosaicking method as in [11] is a powerful framework.

This work also tends to confirm the superiority of our random pattern (III) over the other arrangements with R,G,B filters, as already stated in [28]. The CFAs giving the worst performances are the ones with high light sensitivity, the CFAs (V) and (VI). The advantage of using them lies in the lower amount of noise appearing in the acquired images, since we have to keep in mind that the noise-free formalization of demosaicking is an ideal scenario that is not met in practice. Thus, it makes sense to use CFAs with higher light sensitivity when the sensor is sensitive to noise, which is an actual trend with the increase of number of pixels for a surface area of the sensor kept constant.

The visual inspection of the demosaicked images provides us with a complementary qualitative analysis of the performances of the CFAs. Two parts of the demosaicked image *Lighthouse* are depicted in Fig. 2. They illustrate, respectively, the two main types of artifacts that occur during demosaicking [3]:

- 1) If energy corresponding to high frequency luminance information is assigned to the chrominance, color fringes appear, as visible in the fence in Fig. 2.
- 2) If energy corresponding to chrominance information is incorrectly assigned to the luminance, some high frequency patterns of luminance appear, as visible on the red buoy in Fig. 2. This effect is called *zipper effect* for the Bayer pattern [3].

It is well-known that the Bayer CFA, and its CMY counterpart, exhibit a particularly high sensitivity to aliasing on horizontal or vertical patterns with high frequency content, like the fence in Fig. 2. The CFA (VI) has the same problem, even more problematic because it occurs on patterns oscillating with a frequency two times lower than the Nyquist frequency. This is due to the 2×2 sparser distribution of the R,G,B filters than with the Bayer CFA. Another manifestation of aliasing for this CFA is visible on the reflection in the top left part of the red buoy, which is yellow and should be white. In the case of the random CFA (III), the aliasing artifacts take the form of a color rainbow-like noise randomly distributed and spread over the fence. Due to its low magnitude and the low sensitivity of the human visual system to such chrominance patterns, these artifacts are less disturbing than the coherent moiré structures that appear with periodic CFAs. For this example of the fence, the CFA (VII) delivers the best result.

Concerning the artifacts that appear on the red buoy in Fig. 2, the Bayer CFA yields an image corrupted by disturbing checkerboard pattern. The patterns that appear with the CFAs (II) and (IV) are less visible. The fine white structures that occur with the CFA (VI) are disturbing, too. The worst result is obtained with the CFA (V), for which the buoy is orangish

red. The artifacts take the form of noise on the edges in the case of the random CFA (III). The CFA (VII) performs at best for this example, too.

In conclusion, these results show that there is a significant margin of possible improvement over the Bayer CFA. The CFA (VII) of Hirakawa *et al.* is attractive: it provides artifacts with low magnitude and low visibility, and it has a higher light sensitivity than the CFA (I) to (IV). The even higher light sensitivity of the CFA (V) and (VI) is obtained at the expense of a significantly degraded image quality.

V. CONCLUSION

In this work, we proposed a new linear framework for image demosaicking, which is based on the minimization of a variational functional under the constraint of consistency with the available raw data. This formalism is linear, hence robust, and generic; to our knowledge, the proposed method is the first that can be applied to images acquired with every CFA without any constraint: the pattern can be periodic or random and the colors arbitrary. It would also be easy to extend the approach to the problem of demosaicking multi-spectral images having more than three bands, e.g. for remote sensing applications. We proposed a simple and stable algorithm to implement our method. Although it is iterative, good results are obtained after a few iterations only.

Our future work will concentrate on the extension of the method to the more realistic situation where the data are corrupted by additive noise. The linearity of the method allows to characterize precisely the characteristics of the noise once it has run through the demosaicking process.

REFERENCES

- [1] B. K. Gunturk, J. Glotzbach, Y. Altunbasak, R. W. Schaffer, and R. M. Mersereau, "Demosaicking: Color filter array interpolation," *IEEE Signal Processing Mag.*, vol. 22, no. 1, pp. 44–54, Jan. 2005.
- [2] B. E. Bayer, "Color imaging array," U.S. Patent 3971 065, July, 1976.
- [3] D. Alleyson, S. Süsstrunk, and J. Herault, "Linear demosaicing inspired by the human visual system," *IEEE Trans. Image Processing*, vol. 14, no. 4, pp. 439–449, Apr. 2005.
- [4] E. Dubois, "Frequency-domain methods for demosaicking of Bayer-sampled color images," *IEEE Signal Processing Lett.*, vol. 12, no. 12, pp. 847–850, Dec. 2005.
- [5] J. Portilla, D. Otaduy, and C. Dorronsoro, "Low-complexity linear demosaicing using joint spatial-chromatic image statistics," in *Proc. of IEEE ICIP*, Sept. 2005.
- [6] R. Lukac and K. N. Plataniotis, "Normalized color-ratio modeling for CFA interpolation," *IEEE Trans. Consumer Electron.*, vol. 50, no. 2, pp. 737–745, 2004.
- [7] S. C. Pei and I. K. Tam, "Effective color interpolation in CCD color filter arrays using signal correlation," *IEEE Trans. Circuits Syst. Video Technol.*, vol. 13, pp. 503–513, 2003.
- [8] B. K. Gunturk, Y. Altunbasak, and R. M. Mersereau, "Color plane interpolation using alternating projections," *Proc. IEEE*, vol. 11, no. 9, pp. 997–1013, Sept. 2002.
- [9] D. R. Cok, "Signal processing method and apparatus for producing interpolated chrominance values in a sampled color image signal," U.S. Patent 4 642 678, 1987.
- [10] J. E. Adams, "Design of practical color filter array interpolation algorithms for digital cameras," in *Proc. of SPIE*, vol. 3028, 1997, pp. 117–125.
- [11] K. Hirakawa and P. J. Wolfe, "Spatio-spectral color filter array design for enhanced image fidelity," in *Proc. of IEEE ICIP*, Sept. 2007.
- [12] R. Lukac and K. N. Plataniotis, "Color filter arrays: Design and performance analysis," *IEEE Trans. Consumer Electron.*, vol. 51, no. 4, pp. 1260–1267, Nov. 2005.

- [13] M. Unser and T. Blu, "Generalized smoothing splines and the optimal discretization of the Wiener filter," *IEEE Trans. Signal Processing*, vol. 53, no. 6, pp. 2146–2159, June 2005.
- [14] L. Condat and A. Montanvert, "Fast reconstruction from non-uniform samples in shift-invariant spaces," in *Proc. of EUSIPCO*, Firenze, Italy, Sept. 2006.
- [15] M. Arigovindan, M. Stühling, P. Hunziker, and M. Unser, "Variational image reconstruction from arbitrarily spaced samples: A fast multiresolution spline solution," *IEEE Trans. Image Processing*, vol. 14, no. 4, pp. 450–460, Apr. 2005.
- [16] C. Vázquez, E. Dubois, and J. Konrad, "Reconstruction of nonuniformly sampled images in spline spaces," *IEEE Trans. Image Processing*, vol. 14, no. 6, pp. 713–725, June 2005.
- [17] Y. Hel-Or, "The canonical correlations of color images and their use for demosaicing," HP Laboratories Israel, Tech. Rep. HPL-2003-164R1, Feb. 2004.
- [18] L. M. Hurvich and D. Jameson, "An opponent-process theory of color vision," *Psychological Review*, vol. 64, pp. 384–404, 1957.
- [19] B. A. Wandell, *Foundations of Vision*. Sinauer Associates, Inc., 1995.
- [20] M. Unser and A. Aldroubi, "A general sampling theory for non-ideal acquisition devices," *IEEE Trans. Signal Proc.*, vol. 42, pp. 2915–2925, 1994.
- [21] J. Duchon, "Splines minimizing rotation-invariant semi-norms in Sobolev spaces," in *Constructive Theory of Functions of Several Variables*. Berlin-Heidelberg: Springer-Verlag, 1977, pp. 85–100.
- [22] M. Unser, "Sampling—50 Years after Shannon," *Proc. IEEE*, vol. 88, no. 4, pp. 569–587, Apr. 2000.
- [23] A. Aldroubi and K. Gröchenig, "Nonuniform sampling and reconstruction in shift-invariant spaces," *SIAM Rev.*, no. 4, pp. 585–620, 2001.
- [24] P. Thévenaz, T. Blu, and M. Unser, "Interpolation revisited," *IEEE Trans. Med. Imag.*, vol. 19, no. 7, pp. 739–758, July 2000.
- [25] M. Unser, "Splines: A perfect fit for signal and image processing," *IEEE Signal Processing Mag.*, vol. 16, no. 6, pp. 22–38, Nov. 1999.
- [26] G. Arfken, "Lagrange multipliers," in *Mathematical Methods for Physicists*, 3rd ed. Orlando, FL: Academic Press, 1985, pp. 945–950.
- [27] W. Hakbusch, *Iterative Solutions of Large Sparse Systems of Equations*. New York: Springer-Verlag, 1994.
- [28] L. Condat, "Random patterns for color filter arrays with good spectral properties," *IEEE Trans. Image Proc.*, submitted.
- [29] T. Kijima, H. Nakamura, J. T. Compton, J. F. Hamilton, and T. E. DeWeese, "Image sensor with improved light sensitivity," U.S. Patent 0268 533, Nov., 2007.
- [30] R. Lukac and K. N. Plataniotis, "Universal demosaicking for imaging pipelines with a RGB color filter array," *Pattern Recognition*, vol. 38, pp. 2208–2212, 2005.
- [31] L. Nai-Xiang, C. Lanlan, T. Yap-Peng, and V. Zagorodnov, "Adaptive filtering for color filter array demosaicking," *IEEE Trans. Image Processing*, vol. 16, no. 10, pp. 2515–2525, Oct. 2007.